UC San Diego

Title

The cAMP-induced G protein subunits dissociation monitored in live Dictyostelium cells by BRET reveals two activation rates, a positive effect of caffeine and potential role of microtubules.

Permalink

Authors

Tariqul Islam, A
Yue, Haicen
Scavello, Margarethakay
et al.

Peer reviewed

The cAMP-induced G protein subunits dissociation monitored in live *Dictyostelium* cells by BRET reveals two activation rates, a positive effect of caffeine and potential role of microtubules.

AFM T. Islam[a], **Haicen Yue**[b], **Margarethakay Scavello**[a], **Pearce Haldeman**[a,c], **Wouter-Jan Rappel**[b], and **Pascale G. Charest**[a,*]

[a]Department of Chemistry and Biochemistry, University of Arizona, Tucson, AZ, 85721-0088, USA.

[b]Department of Physics, University of California–San Diego, La Jolla, CA, 92093, USA.

[c]Present address: Division of Biology and Biological Engineering, Joint Center for Transitional Medicine, California Institute of Technology, Pasadena, CA, 91125.

Abstract

To study the dynamics and mechanisms controlling activation of the heterotrimeric G protein Gα2$\beta\gamma$ in *Dictyostelium* in response to stimulation by the chemoattractant cyclic AMP (cAMP), we monitored the G protein subunit interaction in live cells using bioluminescence resonance energy transfer (BRET). We found that cAMP induces the cAR1-mediated dissociation of the G protein subunits to a similar extent in both undifferentiated and differentiated cells, suggesting that only a small number of cAR1 (as expressed in undifferentiated cells) is necessary to induce the full activation of Gα2$\beta\gamma$. In addition, we found that treating cells with caffeine increases the potency of cAMP-induced Gα2$\beta\gamma$ activation; and that disrupting the microtubule network but not F-actin inhibits the cAMP-induced dissociation of Gα2$\beta\gamma$. Thus, microtubules are necessary for efficient cAR1-mediated activation of the heterotrimeric G protein. Finally, kinetics analyses of Gα2$\beta\gamma$ subunit dissociation induced by different cAMP concentrations indicate that there are two distinct rates at which the heterotrimeric G protein subunits dissociate when cells are stimulated with cAMP concentrations above 500 nM versus only one rate at lower cAMP concentrations. Quantitative modeling suggests that the kinetics profile of Gα2$\beta\gamma$ subunit dissociation results from the presence of both uncoupled and G protein pre-coupled cAR1 that have differential affinities for cAMP and, consequently, induce G protein subunit dissociation through different rates. We suggest that these different signaling kinetic profiles may play an important role in initial chemoattractant gradient sensing.
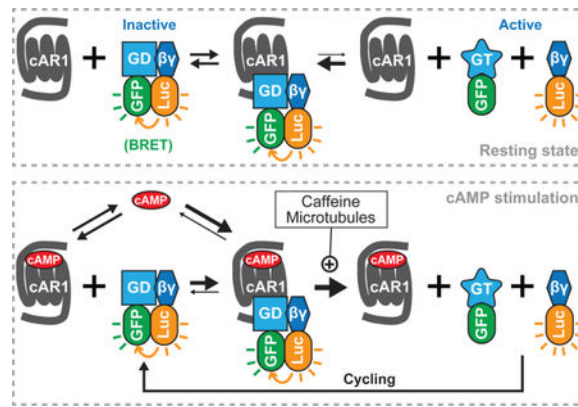
Graphical Abstract

[*]Corresponding author: pcharest@email.arizona.edu.

Conflict of interest
The authors declare that they have no conflicts of interest with the content of this article.

1. Introduction

Chemotaxis, the ability of cells to sense gradients of chemicals (chemoattractants) and migrate towards their highest concentration, is a cellular behavior central to the embryonic development and immune response and that is deregulated in diseases such as cancer metastasis and inflammatory disorders. However, how cells detect and determine the direction of a chemoattractant gradient is not fully understood. Many chemoattractants are detected by seven transmembrane receptors that signal through heterotrimeric G proteins (G protein-coupled receptors; GPCRs), and studies with the chemotaxis experimental model *Dictyostelium discoideum* have provided important insight into chemoattractant GPCR signaling dynamics [1,2]. When food is abundant, *Dictyostelium* is in the growth (or vegetative) stage and grows as single undifferentiated cells [3]. Upon starvation, *Dictyostelium* enters a multicellular development/differentiation program going through aggregation (~4–8 h), mound (~12 h), slug (~16 h), and culmination (~18–24 h) stages that end with the formation of a fruiting body containing spores. Aggregation is mediated by the chemotaxis of cells towards cyclic AMP (cAMP). *Dictyostelium* has four cAMP receptors (cARs) [4,5]. cAR1 expression is maximal during aggregation and cAR3 levels rise towards the end of aggregation, whereas cAR2 and cAR4 are maximally expressed during the slug and culmination stages, respectively [6–9]. There is little cAR expressed in undifferentiated vegetative cells. cAR1 and cAR3 are most similar, with 56% amino acid identity, and they both mediate the response to cAMP through the heterotrimeric G protein Gα2βγ. Although the two receptors display similar cAMP binding affinities in phosphate buffer, cAR3 is ~100 times less efficient than cAR1 in inducing cAMP-stimulated responses and cAR1 is essential for chemotaxis-driven aggregation through Gα2βγ [4,9,10]. Whereas there are twelve G alpha protein subunits in *Dictyostelium*, Gα2 (gene *gpab*) is the main G alpha subunit responsible for the chemotactic responses to cAMP and there is only one G beta (gene *gpba*) and gamma subunit (gene *gpga*) [11–16].

The dynamics and mechanisms controlling cAR1-Gα2βγ coupling are not completely understood. The interaction between Gα2 and Gβγ in live cells has previously been studied using a molecular proximity assay based on Förster (or fluorescence) resonance energy transfer (FRET) and has shown that the G protein subunit dissociation reflects their activation [17]. To investigate the dynamics of cAMP-induced Gα2βγ activation, we have used a similar molecular proximity method, but based on bioluminescence resonance energy transfer (BRET), which we have recently adapted for use in *Dictyostelium* [18]. BRET is similar to FRET but functions with a bioluminescent enzyme (luciferase) as energy donor and, consequently, does not suffer from problems related to fluorescence excitation as in FRET [19]. Several BRET methods have been developed, which differ in the use of different luciferases, luciferase substrates, and fluorescent acceptor proteins [19,20]. We have used the BRET[2] method with the *Renilla* luciferase variant 2 (*R*luc2) and GFP variant 2 (GFP[2]) [21,22]. We show that Gα2GFP[2] and *R*luc2Gβ are functional, that the BRET[2] signal detected in cells expressing both constructs reflects the interaction between the two G protein subunits, and that they behave as previously reported in experiments using FRET [17]. Our studies confirm that cAR1 is the main cAR mediating the cAMP-induced activation of Gα2βγ, with negligible role of cAR3, and show that cAR1 induces Gα2βγ subunit dissociation to a similar extent in both undifferentiated and 5.5 h-differentiated cells. Interestingly, we observed that caffeine, which is commonly used to inhibit cAMP production and autocrine stimulation of *Dictyostelium* cells, increases the potency of cAMP to induce G protein subunit dissociation. Moreover, we found that disturbing the microtubule network but not F-actin inhibits the cAMP-induced Gα2βγ subunit dissociation, suggesting that microtubules facilitate coupling of cAR1 to the heterotrimeric G protein. Finally, kinetics analyses of the cAMP-induced Gα2βγ subunit dissociation responses indicate that elevated cAMP concentrations induces cAR1-dependent G protein dissociation through two distinct rates. Coupled to quantitative modeling, our observations lead us to propose that the two rates come from the presence of both uncoupled and Gα2βγ-pre-coupled cAR1 in resting cells, which have differential affinities for cAMP, and contribute to the initial response of cells exposed to elevated cAMP concentrations through distinct kinetics.

2. Materials and methods

2.1. Reagents

cAMP sodium salt monohydrate, 2'-deoxyadenosine-5'-monophosphate (2'-dcAMP) disodium salt, caffeine powder and anti-Flag M2 were from Sigma-Aldrich (St. Louis, MO, USA). 8-Bromo-cAMP from Enzo Life Sciences (Farmingdale, NY, USA). Coelenterazine 400a was purchased from Biotium (Fremont, CA, USA) and coelenterazine h was obtained from VWR (Radnor, PA, USA). Latrunculin A (Molecular Probes Invitrogen), Benomyl (Chem Service Inc) and Geneticin (GIBCO) were purchased from Thermo Fisher Scientific (Waltham, MA, USA). The Living Colors® GFP monoclonal antibody was purchased from Clontech (now Takara Bio USA Inc.; Mountain View, CA, USA) and the anti-Renilla luciferase antibody clone 5B11.2 was purchased from Millipore SIGMA (Darmstadt, Germany). HRP-conjugated secondary antibodies were purchased from Jackson ImmunoResearch Laboratories, Inc. (West Grove, PA, USA). The cAR1 antibody was a generous gift from Peter Devreotes (Johns Hopkins, Baltimore, MD) and is described

elsewhere [23]. GFP-Tubulin and the extra-chromosomal vector pDM304 and pDM344 were obtained through the Dicty Stock Center, deposited by Doug Robinson (Johns Hopkins, Baltimore, MD) and Douwe Veltman, respectively [24–26]. Gα2-CFP/pDM358 and Gβ cDNA were gifts from Chris Janetopoulos (University of the Sciences, Philadelphia, PA) and described elsewhere [17]. The *Renilla* luciferase variant 2 (*R*luc2; [21]) and GFP variant 2 (GFP[2]) were gifts from Michel Bouvier (Universite de Montréal, Montréal, Canada). The Lifeact-GFP construct was a gift from Rick Firtel (University of California–San Diego, La Jolla, CA) and was previously described [27–29].

2.2. Cell culture and strains used

Dictyostelium cells were grown attached to substrate in axenic HL5 medium including glucose (ForMedium, Hunstanton, Norfolk, UK) at 22°C and transformants were generated by electroporation. Transformed cells were selected in 20 μg/ml Geneticin and expression confirmed by immunoblot. Cells were differentiated by pulsing with 30 nM cAMP every 6 min for 5.5 h in 12 mM Na/K phosphate pH 6.1 at a confluency of $5X10^6$ cells/ml. The wild-type cells used are AX3. *ga2* (*gpaB*), *gβ* (*gpbA*), and *carC*⁻ mutant cells were obtained from the Dicty Stock Center where they were deposited by Peter Devreotes (Johns Hopkins, Baltimore, MD) and described elsewhere [6,25,30]. The *carA*⁻ cells were generously provided by Alan Kimmel (NIH, Bethesda, MD) and the *carA*⁻*carC*⁻ cells (clone RI9) were a gift from Chris Janetopoulos and were both previously described [31,32].

2.3. DNA constructs and validation

All DNA constructs were generated with standard molecular cloning techniques. To make Gα2GFP[2]-pDM304, CFP in Gα2CFP-pDM358 was replaced by GFP[2] after residue 90 of the Gα2 cDNA, using the SpeI restriction sites, and the hygromycin resistance cassette of pDM358 was replaced with the neomycin cassette from pDM304 by subcloning using restriction sites BamHI and XhoI. To make *R*luc2Gβ, *R*luc2 was first cloned into the BglII restriction site of shuttle vector pDM344, eliminating the BglII site on the C-terminal end of *R*luc2 by ligating to a compatible BamHI site. Gβ was then cloned in C-terminal of *R*luc2 with the addition of a 4 amino acid linker (GSGS) using restriction sites BglII and Spe1. The *R*luc2Gβ-containing NgoMIV cassette of pDM344 was subcloned into pDM304 and Gα2GFP[2]-pDM304 at the NgoMIV site, to generate *R*luc2Gβ-pDM304 and *R*luc2Gβ-Gα2GFP[2]-pDM304, respectively.

Primers sequences were as follows:

GFP[2] forward, AAGTGACTAGTATGGTGAGCAAGGGCGAGGAGCTG;

GFP[2] reverse, AAGTGACTAGTCTTGTACAGCTCGTCCATGC;

*R*luc2 forward, AAGTGGGATCCAAAAAATGACAAGTAAAGTTTACGACCCCGAGCAGAGG;

*R*luc2 reverse, AAGTGAGATCTACCAGAACCACCCTGCTCGTTCTTCAGCACTCTC;

Gβ forward,
AAGTGAGATCTATGTCATCAGATATTTCAGAAAAAATTCAACAA
GCAAGAAGAG;

Gβ reverse, AAGTGACTAGTTTAAGCCCAAATCTTGAGGAGAGAATCC.

The BRET constructs were verified by sequencing and validated as previously described [18]. Briefly, expression and integrity of the fusion constructs was verified by immunoblot using *R*luc and GFP antibodies according to the manufacturer protocol; *R*luc2 and GFP^2 functionality was verified by assessing luminescence with coelenterazine h at 480 nm and fluorescence at 510 nm, respectively, using a POLARstar Omega microplate reader (BMG Labtech, Ortenberg, Germany); and functionality of Gα2GFP^2 and *R*luc2Gβ was verified by assessing rescue of the aggregation defects of *ga2$^-$* and *gβ$^-$*, respectively, by plating Gα2GFP^2/*ga2$^-$* and *R*luc2Gβ/*gβ$^-$* cells on 12 mM Na/K phosphate agar plate and tracing the cells' development using a dissection microscope.

2.4. BRET^2 Assay and data analysis

The BRET^2 assay was performed as previously described [18]. Briefly, 1.5×10^6 cells was mixed with 5 μM final Coelenterazine 400a in a 96-well white microplate. The BRET^2 signal was detected using a POLARstar Omega microplate reader (BMG Labtech, Ortenberg, Germany) by simultaneously measuring light through 370–450 nm and 500–530 nm filters. BRET^2 measurements were taken before and after injection of stimuli, where indicated, every 0.5 s at 22 °C. Injection of 12 mM Na/K phosphate buffer was used as control. For each measurement, the GFP^2 fluorescence signal detected at 500–530 nm was divided by the *R*luc2 emission signal detected at 370–450 nm to calculate the BRET^2 ratio. The BRET^2 ratio obtained with cells expressing only *R*luc2Gβ (background control) was subtracted from that of cells expressing both *R*luc2Gβ and Gα2GFP^2 to calculate the "net BRET^2". BRET^2 and net BRET^2 were then multiplied by 1000 to express the data as milli-BRET units (mBU). Where indicated, cells were pretreated with 5 μM Latrunculin A for 15 min, or 50 μM Benomyl for 15 min before they were used in the BRET^2 assay. The drugs were initially diluted in DMSO, which was at 0.5 % final concentration after dilution. 0.5 % DMSO in 12 mM Na/K phosphate buffer was then used as control. Cells were stimulated with the indicated final concentrations of cAMP in the presence of 10 mM DTT, diluted in 12 mM Na/K phosphate buffer. DTT is used to inhibit cell-secreted phosphodiesterases and prevent cAMP degradation [33], which could significantly change the cAMP concentration cells are exposed to, especially when using low doses. Dose-responses and kinetics analyses were performed using Prism (GraphPad Software Inc.) and MATLAB (MathWorks), respectively.

2.5. Imaging

Contrast images of developing cells were taken with a Motic digital dissecting microscope. DIC and fluorescence images were acquired using a Marianas Spinning Disk Confocal Workstation (Intelligent Imaging Innovations, In., Denver, CO, USA) equipped with an Evolve™ 512 EMCCD camera (Photometrics, Tucson, AZ, USA), and image analysis was performed using the Slidebook software (Intelligent Imaging Innovations, Denver, CO,

USA). Where indicated, cells were treated with 5 μM Latrunculin A for 15 min or 50 μM Benomyl for 15 min before imaging.

2.6. Kinetics analyses

The net $BRET^2$ data was normalized using the average basal net $BRET^2$ measured before stimulation for each condition, which was set to 1. The net $BRET^2$ data were then fitted using the single exponential function: $BRET^2 = 1 + a(e^{-rt} - 1)$ or double exponential function: $BRET^2 = 1 + a_1\left(e^{-r_1 t} - 1\right) + a_2\left(e^{-r_2 t} - 1\right)$. Residuals of fitting are calculated by subtracting the data from the predicted values of the fit. To quantitatively determine the best fit, the error difference between single and double exponential fit was calculated as $\Delta E = \dfrac{RMSE_1 - RMSE_2}{RMSE_2}$, where $RMSE_1$ is the root mean squared error of the single exponential fit and $RMSE_2$ is that of the double exponential fit. From our analyses, we determined that a $\Delta E < 0.05$ indicates that the data can be fitted with a single exponential and a $\Delta E > 0.1$ indicates a double exponential function provides the best fit. A ΔE between 0.05 and 0.1 is ambiguous, meaning that the data could be fitted as well using a single or double exponential function. Every time curve obtained for different cAMP concentration was fitted using this standard, generating corresponding rates r (single rate) or r_1 and r_2 (two rates).

2.7. Computational modeling

Six reactions were considered to model the cAMP receptor coupling to and activation of heterotrimeric G protein Gα2βγ. The first reaction is the basal level of receptor (R) pre-coupled to the inactive, GDP-bound heterotrimeric G-protein (GD) in the absence of cAMP ligand (L), with rates k_1 and k_{-1}. The equation for pre-coupled receptor (RGD) without cAMP is defined as:

$$\frac{d[RGD]}{dt} = k_1[R][GD] - k_{-1}[RGD]$$

Without ligand, $[R] = R^{tot} - [RGB]$ and $[GD] = G^{tot} - [RGB]$. Consequently, the stable value of [RGD] before adding L is obtained by setting $\frac{d[RGD]}{dt} = 0$, and this is also the initial value for [RGD] after L is added:

$$[RGD]_{initial} = \frac{R^{tot} + G^{tot} + K_1 - \sqrt{\left(R^{tot} + G^{tot} + K_1\right)^2 - 4G^{tot}R^{tot}}}{2}$$

$K_1 = \dfrac{k_{-1}}{k_1}$ is the equilibrium dissociation constant and its reciprocal $\dfrac{1}{K_1}$ represents the binding affinity between R and GD. The second reaction is where L binds RGD to form LRGD, with rates k_2 and k_{-2}. The third reaction is where L binds R to form LR, with rates k_3 and k_{-3}. The fourth reaction is where LR then binds GD to form LRGD, with rates k_4 and k_{-4}. The fifth reaction is where the heterotrimeric G protein becomes active, GTP-bound (GT, with Gα2 and Gβγ subunits dissociated) and dissociates from the receptor to form LR + GT. In

Dictyostelium cells exposed to cAMP, because heterotrimeric G protein subunits don't adapt and display a steady state of activation as long as the stimulus is present (this study and [17]), we assume that this reaction is irreversible in the conditions used, with rate k_5. The sixth reaction is considering the cycling of GT back to GD with re-association of the Gα2 and Gβγ subunits upon GTP hydrolysis, which can then bind R or LR again, with rate k_6. To quantitatively explain the observed dissociation kinetics and represent the whole activation/deactivation cycle of the heterotrimeric G protein, the following 4 ordinary differential equations were used:

$$\frac{d[RGD]}{dt} = k_1 \left(R^{tot} - [RGD] - [LR] - [LRGD] \right)\left(G^{tot} - [RGD] - [LRGD] - [GT] \right)$$
$$+ k_{-2}[LRGD] - k_2[RGD][L] - k_{-1}[RGD]$$

$$\frac{d[LR]}{dt} = k_3[L]\left(R^{tot} - [RGD] - [LR] - [LRGD] + k_{-4}[LRGD] + k_5[LRGD] - k_{-3}[LR] \right)$$
$$- k_4[LR]\left(G^{tot} - [RGD] - [LRGD] - [GT] \right)$$

$$\frac{d[LRGD]}{dt} = k_2[RGD][L] + k_4[LR]\left(G^{tot} - [RGD] - [LRGD] - [GT] - k_{-2}[LRGD] \right)$$
$$- k_{-4}[LRGD] - k_5[LRGD]$$

$$\frac{d[GT]}{dt} = k_5[LRGD] - k_6[GT]$$

These equations were normalized for $R^{tot} = 1$, leaving 11 independent parameters. For every value of [L], the equations were solved and the value $\frac{G^{tot} - [GT]}{G^{tot}}$ are compared to the normalized experimental data. The same procedure and standard as those for fitting the experimental data with single and double exponential functions were then used to obtain the exponential rates (r or r_1 and r_2) and amplitude of the response (a or $a_1 + a_2$) for the simulation results. These rates and amplitudes for different [L] are then fitted to experimental data to identify proper values for the 11 parameters. This fitting was carried by employing a simulated annealing method, using the simulannealbnd function in MATLAB(R2015b) with default settings, as we previously reported [34,35]. First, an error function was defined as:

$$\text{Error} = \sum_i W_1\left(r_{1i}^s - r_{1i}^e\right)^2 + W_2\left(r_{2i}^s - r_{2i}^e\right)^2 + W_3\left(a_{1i}^s + a_{2i}^s - a_{1i}^e - a_{2i}^e\right)^2$$

r_1, r_2, a_1, and a_2 are the exponential rates and response amplitudes obtained from a double exponential fit. When a single exponential fit is good, we set $r_1 = r_2 = r$ and $a_1 = a_2 = \frac{a}{2}$, where r and a are obtained from a single exponential fit. Subscript "i" represents the ith

group with [L] = [L]$_i$. W is the weight of different terms that can be tuned. Superscript "s" means simulation results and "e", experimental results. The simulated annealing prevents trapping the fit in a local minimum by accepting a trial step with some probability dependent on an artificial temperature T, even when this step does not improve the fit. The initial temperature was set to be high to allow for a larger searching area. Then, the temperature was gradually decreased, leading to more selective sampling towards the error decreasing direction. The position in the parameter space where the error function is minimal for each of the 11 parameters in the model was then determined: $k_1 = 0.002$; $K_1 = 0.962$; $k_2 = 0.007$; $K_2 = 1.24$; $k_3 = 0.502$; $K_3 = 78.4$; $k_4 = 0.214$; $K_4 = 1.04$; $k_5 = 0.905$; $k_6 = 0.075$; $G^{tot} = 0.989$. To simulate the heterotrimeric G protein subunit dissociation rates in the absence of pre-coupled receptors (RGD), the initial value for RGD was set to zero in the ODEs indicated above.

2.8. Statistics

Results are expressed as the mean of at least three independent experiments. Error bars represent SD for bar graphs and SE for dose-response curves. Statistical analysis was performed using the one-way ANOVA test.

3.   Results and discussion

3.1.   Gα2 and Gβ subunits dissociation monitored by BRET^2

To study heterotrimeric G protein activation in *Dictyostelium* by monitoring the interaction between the Gα2 and Gβγ subunits using BRET^2, we used the *Renilla reniformis* luciferase variant 2 (*R*luc2) and the BRET^2 energy acceptor GFP^2 [21,22]. We fused the luciferase in frame at the N-terminus of Gβ and inserted GFP^2 into the first loop of the helical domain of Gα2, based on previously reported and validated fluorescent protein constructs of Gα2 [17]. To first determine if the Gα2GFP^2 and *R*luc2Gβ constructs are functional, we expressed them individually in *Dictyostelium* cells lacking Gα2 (*ga2⁻* cells) and Gβ (*gβ⁻* cells), respectively. *ga2⁻* and *gβ⁻* cells are unable to aggregate and undergo development but expression of exogenous Gα2 or Gβ can rescue the developmental defects [14,16], which can then be used as a readout to determine if Gα2 or Gβ constructs are functional. We observed that expression of Gα2GFP^2 and *R*luc2Gβ in their respective null mutant strains rescues the ability of these cells to aggregate and develop into fruiting bodies, although not as numerous and large as those produced by wild-type cells (Fig. 1A). This is likely due to the fact that not all the cells express the constructs. Nonetheless, because expression of Gα2GFP^2 and *R*luc2Gβ in their respective null mutant strain generates cells that are able to aggregate and develop indicates that the constructs are at least partly functional. Because we planned on using *ga2⁻* cells for the BRET assays, we then expressed Gα2GFP^2 and *R*luc2Gβ constructs together or *R*luc2Gβ alone, which will serve as the background BRET control, in *ga2⁻* cells. The co-expression of Gα2GFP^2 with *R*luc2Gβ rescues the *ga2⁻* cells developmental defects similarly to Gα2GFP^2 expression alone, indicating recovery of G protein signaling in these cells (Fig. 1A). Immunoblotting of cell lysates revealed proteins with apparent molecular weights of ~ 70 kDa for Gα2GFP^2 [calculated 71.9 kDa (Gα2, 43.6 kDa and GFP^2, 28.3 kDa)] and ~ 75 kDa for *R*luc2Gβ [calculated 78.7 kDa (Gβ, 40.9 kDa, and *R*luc2, 37.8 kDa)], respectively, indicating the successful expression of the expected

fusion proteins in both $ga2^-$ and wild-type cells (Fig. 1B, S1A). In addition, cells expressing Gα2GFP[2] or Rluc2Gβ produce significant, above background fluorescence and luminescence signals, respectively, indicating properly folded and functional GFP[2] and luciferase moieties (Fig. 1C). Of note, we observed that the background luminescence and fluorescence signals in non-transformed WT and $ga2^-$ cells are considerably different in undifferentiated and 5.5 h-differentiated cells. The decrease in background fluorescence in 5.5 h-differentiated cells is actually consistent with a previous report showing that incubation of cells in phosphate buffer decreases autofluorescence that comes from vitamins in the growth medium [36]. However, we also observed an unexpected increase in the background luminescence signal in 5.5 h-differentiated cells compared to undifferentiated cells. This increase in luminescence indicates an increase in basal coelenterazine oxidation, in the absence of luciferase, and we believe that this is due to elevated superoxide production in developing *Dictyostelium* cells [37]. Nonetheless, altogether, our results indicate that the Gα2GFP[2] and Rluc2Gβ fusion constructs are functional.

To monitor the interaction between the two G protein subunits by BRET[2], we used 5.5 h-differentiated Gα2GFP[2]/Rluc2Gβ-expressing $ga2^-$ cells and $ga2^-$ cells expressing only Rluc2Gβ, to levels equivalent to those of cells expressing both constructs, to determine the background BRET[2] signal. When the two proteins were co-expressed, we detected a specific BRET[2] signal (62.6 ± 0.3 mBU) of ~ 3 fold over background detected in Rluc2Gβ/$ga2^-$ cells (22.8 ± 0.4 mBU), indicative of the interaction between Gα2GFP[2] and Rluc2Gβ (Fig. 2A). To assess the effect of cAMP stimulation on the G protein subunit interaction, we injected a saturating dose of cAMP (10 μM) while monitoring the BRET[2] signal in real-time before, during and after cAMP injection. We observed that cAMP stimulation leads to a rapid loss in the BRET[2] signal detected in Gα2GFP[2]/Rluc2Gβ/$ga2^-$ cells, up to ~30–40 decrease in total BRET[2] signal (63 to 36 mBU; Fig. 2A) reaching a steady state approximately 20 s after stimulation (Fig. 2B). cAMP stimulation of cells expressing Rluc2Gβ alone (Fig. 2A) or the injection of buffer to Gα2GFP[2]/Rluc2Gβ-expressing cells (Fig. 2B) has no effect, suggesting that the observed cAMP-induced decrease in BRET[2] signal in Gα2GFP[2]/Rluc2Gβ/$ga2^-$ cells reflects the cAMP-induced activation and dissociation of the heterotrimeric G protein subunits.

To further confirm that the Gα2GFP[2] and Rluc2Gβ can be used to study heterotrimeric G protein activation, we assessed their dissociation in response to different concentrations of cAMP. We observed a dose-dependent decrease in BRET[2] signal between Gα2GFP[2] and Rluc2Gβ, with a measured EC50 of ~29 nM (Fig. 2C). This EC50 is similar to the K_d of the high affinity binding site of cAMP on cAR1 (~30 nM) for cells in a phosphate buffer similar to that we used in our experiments [4]. This is interesting because the cAR1 high affinity site was reported to represent only ~5–10% of the cAR1 population expressed during aggregation, with the remaining 90–95% having lower affinity (K_d of ~300 nM) [4,39]. It is possible, though, that the overexpression of the heterotrimeric G protein subunits affects this proportion and that there are more high affinity binding sites in the transformed cells. Nonetheless, the observation that the cAMP-induced G protein dissociation EC50 is ~29 nM while stimulation with 250 nM cAMP almost inducing a full response, and 500 nM inducing the full response, suggests that the high affinity cAR1 sites (K_d ~30 nM) are the main mediators of cAMP-induced G protein subunits dissociation.

Of note, this cAMP-induced G protein dissociation EC50 is slightly greater than what we previously reported in our recent BRET method article [18] as well as what was previously found for the G protein dissociation detected by FRET (~10 nM) [17]. The difference is that we and the other authors had previously pretreated the cells with caffeine to inhibit the production of cAMP and its autocrine stimulation of cells. To then directly assess if caffeine affects the cAMP-induced G protein dissociation, we treated our cells with 5 mM caffeine before measuring the change in BRET^2 upon cAMP stimulation. Interestingly, we observed that, in cells treated with caffeine analyzed in parallel to untreated cells, cAMP induces Gα2$\beta\gamma$ subunits dissociation to a similar extent but with a significantly increased potency, with a measured half maximal effective concentration (EC50) of ~4 nM (Fig. 2C). Therefore, our observation suggests that caffeine increases the potency of cAMP to induce Gα2$\beta\gamma$ dissociation We do not know the mechanism underlying the effect of caffeine on G protein dissociation, but a previous study of cAMP binding on whole cells showed that 10 mM caffeine leads to a conversion of most binding sites to the low affinity conformation [40]. Therefore, although we used a little less caffeine (5 mM) in our assay, it is unlikely that caffeine increases the potency of cAMP-induced Gα2$\beta\gamma$ subunit dissociation by increasing the cAMP binding affinity. Caffeine inhibits cAMP production in *Dictyostelium* [41]. Consequently, the treatment of cells with caffeine became a popular method of preventing the autocrine stimulation of cells and, thereby, reducing the basal levels of biochemical activities in cells to facilitate their measurement in response to acute cAMP stimulation. Whereas the mechanism of action of caffeine in *Dictyostelium* remains to be defined, our observation suggests that it affects more than just the autocrine stimulation of cells.

We also assessed G protein dissociation in response to the two well-characterized cAMP analogs, 2'-deoxy cAMP (2'-dcAMP) and 8-bromo cAMP (8-Br-cAMP) in the presence of caffeine as previously reported [17]. We measured EC50s of ~17 nM for 2'-dcAMP and ~3 μM for 8-Br-cAMP, similar to the previously reported values (Fig. 2C). Therefore, these results, together with the cAMP-induced dissociation of Gα2$\beta\gamma$ subunits, are consistent with previous observations of Gα2$\beta\gamma$ subunit dissociation monitored by FRET [17]. In this study, Janetopoulos *et al.* also demonstrated that the cAMP-induced activation and dissociation of the Gα2$\beta\gamma$ subunits does not adapt to continuous stimulation. Instead, the G protein subunits reach a steady state of dissociation/activation as long as the stimulus is present, and after clearing of the cAMP the heterotrimeric G protein can be re-stimulated. Consistent with these previous findings, we observed that the loss of BRET^2 signal between Gα2GFP^2 and *R*luc2Gβ upon stimulation of the cells with a saturating dose of cAMP persists as long as the stimulus is present (Fig. 2D). The BRET^2 signal is fully recovered when the stimulus is washed away, and the cells then respond to a re-stimulation with an equally effective loss of BRET^2 signal, indicating that the heterotrimeric G protein subunits re-associated upon removal of cAMP and re-dissociated upon application of the second stimulus. Altogether, our results indicate that the Gα2GFP^2 and *R*luc2Gβ constructs are functional and, when expressed together, the resulting BRET^2 signal serves as readout of their interaction in live cells, which can then be used to study Gα2$\beta\gamma$ activation.

3.2. cAR1 mediates the cAMP-induced activation of Gα2βγ in undifferentiated and differentiated cells.

Previous observations suggest that cAMP induces activation of some chemotactic pathways in undifferentiated cells as efficiently as in aggregation-competent cells [42]. To further investigate this, we compared the cAMP-induced activation of Gα2βγ in undifferentiated and 5.5 h-differentiated, aggregation-competent cells. We detected similar basal net BRET^2 signals in both undifferentiated and 5.5 h-differentiated Gα2GFP^2/*R*luc2Gβ/*ga2⁻* cells, suggesting that a comparable proportion of Gα and βγ subunits are interacting in resting conditions, independently of the cells' developmental stage (Fig. 3A). Interestingly, we observed that cAMP stimulation of undifferentiated cells induces G protein subunits dissociation to similar extent and potency as that observed in 5.5 h-differentiated cells, with the same effect of caffeine on the EC50 (Fig. 3A and B). In addition, we observed similar cAMP-induced G protein subunits dissociations when expressing Gα2GFP^2 and *R*luc2Gβ in wild-type cells, although the basal net BRET^2 signal in 5.5 h-differentiated wild-type cells was lower compared to undifferentiated wild-type cells (Fig. 3C).

The difference in basal net BRET^2 signal between undifferentiated and 5.5 h-differentiated wild-type cells could partly be due to the considerable reduction in Gα2GFP^2 expression in differentiated wild-type cells compared to the undifferentiated cells, as detected by the decrease in fluorescence (Fig. 1C). This could also be due to the much increased cAR1 expression in differentiated wild-type cells, leading to increased basal Gα2βγ activity and dissociated subunits, which is not observed in the *ga2⁻* cells possibly because they have reduced cAR1 expression [14] (Fig. S2). In addition, the finding that cAMP stimulation of undifferentiated cells induces G protein subunit dissociation and, thus, activation, to the same extent as to that in 5.5 h-differentiated cells was unexpected. Although it is possible that overexpressing the G protein subunits disrupts the relative expression levels of other signaling components, cAR1 expression in undifferentiated cells is not increased as a result of Gα2GFP^2 and *R*luc2Gβ expression (Fig. S2). As expected, we observed that cAR1 expression is equally very low in undifferentiated cells expressing or not Gα2GFP^2 and *R*luc2Gβ, whereas cAR1 is strongly increased in 5.5 h-differentiated wild-type cells. As previously reported, we observed that *ga2⁻* cells express much less cAR1 than wild-type cells, even after cAMP pulsing for 5.5 h, [43] and that expression of Gα2GFP^2 and *R*luc2Gβ restores some of the cAR1 expression in differentiated *ga2⁻* cells, but to levels that remain considerably low. Therefore, our observations suggest that the low cAR1 expression levels in undifferentiated cells, and in *ga2⁻* cells expressing Gα2GFP^2 and *R*luc2Gβ, are sufficient to fully activate Gα2βγ in response to cAMP. Consequently, it is intriguing why cAR1 expression levels increase so much during aggregation (according to reported cAR1 mRNA levels: ~100 times more for cells growing on bacteria and developed on filters and ~1000 times more for axenic cells developed by cAMP pulsing) [6,44], which is believed to be essential for efficient chemotaxis to cAMP.

Since both cAR1 and cAR3 couple to Gα2βγ, we assessed the contribution of both of these receptors to the measured cAMP-induced dissociation of Gα2βγ in undifferentiated versus differentiated cells. We expressed Gα2GFP^2 and *R*luc2Gβ in cells lacking cAR1 (*carA⁻* cells) and/or cAR3 (*carC⁻* and *carA⁻carC⁻* cells), as well as in wild-type cells to use as

control, and assessed the effect of cAMP stimulation on the BRET^2 signal. We observed that stimulation with a saturating cAMP concentration (10 μM) of cells lacking cAR1 fails to induce considerable G protein subunit dissociation, whereas cells lacking only cAR3 display G protein subunit dissociation comparable to that in wild-type cells in both extent and potency (Fig. 3C and 3D). These results indicate that, in both undifferentiated and 5.5 h-differentiated cells, the detected cAMP-induced dissociation of Gα2βγ results from cAR1 stimulation, and that cAR3 must be expressed at levels too low to significantly contribute to the this response in the conditions used.

3.3.   Disrupting microtubules inhibits G protein subunit dissociation

A previous study showed that disrupting the actin cytoskeleton increases the mobility of cAR1 at the plasma membrane, whereas microtubule disruption inhibits cAR1's mobility and its mediated production of phosphatidylinositol 3,4,5-triphosphate [PI(3,4,5)P$_3$] in response to cAMP stimulation [45]. These observations suggested that the potential anchoring of cAR1 to microtubules is important for proper cAR1 signaling. To assess the effect of disrupting actin and microtubules on the cAR1-induced activation and dissociation of Gα2βγ, we treated cells with the actin polymerization inhibitor Latrunculin A (LatA) [46] and the microtubule destabilizer Benomyl as previously reported [45]. Benomyl is a bioactive benzimidazole that, like nocodazole, specifically inhibits microtubule assembly by binding to tubulin subunits [47], but its effects on *Dictyostelium* were shown to be less severe than other microtubule destabilizers [48]. As expected, LatA and Benomyl treatment of cells leads to a loss of morphological cell polarity due to the disruption of F-actin and microtubule network, as observed using the F-actin reporter Lifeact-GFP and γ-tubulin-GFP, respectively (Fig. 4A and B). Disrupting actin or microtubules did not affect the interaction of Gα2 with βγ in resting cells, as observed by similar basal BRET^2 signals (Fig. 4C). Interestingly, whereas the LatA-mediated disruption of F-actin did not significantly affect the extent and potency of cAMP-induced G protein subunit dissociation, compared to vehicle (0.5% DMSO)-treated control cells, the Benomyl-mediated disruption of microtubules considerably inhibited G protein subunit dissociation (Fig. 4C and D). Note that treatment of cells with 0.5% DMSO produced a left-shift in the dose-response curve compared to non-treated cells, similar to the effect of caffeine. We don't know how DMSO affects G protein dissociation. Nonetheless, although additional studies will be necessary to properly define the role of the cytoskeleton in G protein activation, our observations suggest that microtubules, and not actin, are important for the cAR1-induced activation of Gα2βγ. These observations are consistent with previous work suggesting that F-actin does not play a significant role in the cAR1 coupling to and activation of Gα2βγ [45,49–51]. Moreover, the observation that intact microtubules are necessary for optimal cAR1-induced Gα2βγ activation provides a possible explanation for the reported dependency of cAMP-induced PI(3,4,5)P$_3$ production on an intact microtubule network [45].

3.4.   Analysis of the cAR1-promoted Gα2βγ dissociation kinetics

To investigate the dynamics of cAMP-induced Gα2βγ activation, we measured G protein subunit dissociation in real-time in response to different cAMP concentrations and compared wild-type to *carC⁻* cells to determine if cAR3 may contribute to the observed kinetics (Fig. 5, S3). Each time curve was fitted using single and double exponential decay and the

goodness of fit was determined as described in the Materials and methods section (Table S1). Interestingly, we found that G protein subunits dissociation induced by cAMP concentrations of ~500 nM and below can be fitted with a single exponential whereas that induced by cAMP concentrations above 500 nM are best fitted with double exponentials with two rates (Fig. 5, S3, Table S1). Similar kinetics were observed using wild-type and *carC-* cells, supporting our previous observation that the detected cAMP-induced Gα2βγ dissociation is mainly due to cAR1 and that the appearance of a second rate at higher cAMP concentrations is not due to cAR3 signaling (Fig. 5). Kinetics analyses of data obtained with Gα2GFP^2/*R*luc2Gβ-expressing *ga2-* cells also show similar results (Fig. S4).

Interestingly, the cAMP concentration at which the presence of a second G protein dissociation rate becomes obvious correlates with cAMP concentrations at which most of the low affinity cAR1 binding sites (K_d~300 nM versus high affinity sites K_d~30 nM) should be occupied [4]. Evidence suggest that the high affinity cAR1 binding sites in *Dictyostelium* are receptors already in complex with the G protein, as is the case for many mammalian GPCRs [16,52–58]. However, whether G protein pre-coupled cAR1 contributes to cAMP signaling is debated [51,59]. To investigate the cAMP-induced Gα2βγ dissociation kinetics profile, we considered a simple model of receptor-G protein coupling, in which both free cAR1 (R) and cAR1 pre-coupled to inactive Gα2βγ (RGD) potentially exist in an equilibrium in resting cells (Fig. 6A). In our model, we postulate that upon stimulation with cAMP ligand (L), the latter can bind to R or RGD to generate LR and LRGD, respectively. In turn, LR then recruits GD to also lead to LRGD. Formation of LRGD stimulates exchange of GDP for GTP on the G protein, thereby activating it leading to LR + GT. In *Dictyostelium*, evidence suggest that the Gα2βγ subunits dissociate upon activation, so we consider that GT = Gα2 + Gβγ [17,49–51]. Upon GTP hydrolysis on Gα2, the subunits then re-associate to form GD that can be activated again as long as cAMP is present. Six reactions total are considered, as shown in Fig. 6A and described under Materials and methods. In our scheme, the appearance of two rates of G protein dissociation for higher cAMP concentrations is due to increased cAMP binding to uncoupled receptors to which it has lower affinity. Our scheme also incorporated that cAMP binding to lower affinity, uncoupled receptors produces a slower G protein activation response due to the additional G protein recruitment step. We generated a quantitative model of this scenario including both uncoupled (R) and pre-coupled receptors (RGD) that can simulate the kinetics data very well (Model R + RGD; Fig. 6B). Using this model, when we simulate the responses in the absence of pre-coupled receptors (Model R), we obtain only one rate throughout the range of cAMP concentrations used, supporting the hypothesis that one of the rates comes from binding to pre-coupled receptors (Model R; Fig. 6B).

In a previous study, Xu *et al.* considered the role of three possible cAR1 coupling mechanisms during chemotaxis: (1) R+GD→RGD+L→LRGD→LR+GT (with receptor pre-coupling); (2) L+R→LR+GD→LRGD→LR+GT (no pre-coupling); and (3) the previous two mechanisms combined (co-existence of uncoupled and pre-coupled receptors) [51]. As their results show that persistent ligand stimulation results in steady-state G protein activation, coupling mechanism (1) was ruled out, as it cannot allow a persistent cycle. However, the model of Xu *et al.* did not allow quantitatively discriminating between mechanisms (2) and (3) and, thus, did not determine whether pre-coupled receptors

contribute to G protein activation during chemotaxis to cAMP. Compared to the model by Xu *et al.*, our model uses fewer intermediate steps, parameters and variables, and does not have any spatial dynamics, which makes it easier to quantitatively fit our experimental data and provide insight into potential coupling mechanisms underlying the two G protein subunits dissociation rates that we observe. Our results suggest that pre-coupled receptors play a role in the rapid activation of the heterotrimeric G protein upon cAMP stimulation. Consequently, our results suggest that mechanism (3) described above, which includes contribution of both uncoupled and pre-coupled receptors, is likely the mechanism for cAMP-induced activation of heterotrimeric G proteins.

To test the prediction that the two cAMP-induced G protein dissociation rates are related to the high and low affinity cAR1 binding sites, we performed an experiment in which we stimulated the cells with two sequential cAMP concentrations. For the first stimuli, we used sub-saturating cAMP concentrations of 10, 20, and 50 nM, and we used a saturating cAMP concentration of 10 μM for the second stimuli (Fig. 6C). We postulated that lower doses of cAMP would preferentially bind and activate high affinity cAR1 sites, reducing the number of high affinity sites available for the second stimulus. Consequently, the double exponential in the G protein dissociation profile from stimulation with 10 μM cAMP would become gradually less obvious as the strength of the first stimulus increases. As an additional control, we also stimulated cells with 10 nM cAMP followed by a second stimulus with sub-saturating cAMP concentration of 300 nM. We analyzed the kinetics of the response after the second stimulus and compared to that obtained with cells directly stimulated with 10 μM cAMP. To determine the best fit for the data, we calculated the error difference (E) between single and double exponential fit. We found that the 10 μM cAMP-induced response has decreasing E as the concentration of the first cAMP stimulus increases (Fig. 6D). On the other hand, the 300 nM cAMP-induced response, following the first 10 nM cAMP stimulation, is fitted equally well with single and double exponentials (Fig. S5). Therefore, these results support the hypothesis that, in resting cells, two cAR1 sites of differential affinities for cAMP underlie the two rates observed when cells are stimulated with elevated, saturating cAMP concentrations.

cAR1 expressing cells have high and low affinity binding sites for cAMP with K_d of ~30 and 300 nM, respectively [4]. Previous observations suggest that the high affinity cAMP binding sites are G protein-dependent [16,57,58]. The cAMP concentrations inducing G protein subunit dissociation through two distinct rates correlate with cAMP concentrations at which both high and low affinity binding sites would be occupied. Therefore, we propose that the kinetics of cAMP/cAR1-induced G protein subunit dissociation that we observe result from the co-existence, in resting cells, of both uncoupled and pre-coupled cAR1 that have differential affinities for cAMP. At cAMP concentrations of ~500 nM and below, mostly high affinity pre-coupled cAR1 sites are occupied and promote Gα2βγ activation, reflected by only one rate of G protein subunit dissociation. However, at cAMP concentrations above 500 nM, both high affinity pre-coupled cAR1 and low affinity uncoupled cAR1 sites are occupied. In this case, pre-coupled cAR1 leads to rapid G protein activation while uncoupled cAR1 first needs to recruit Gα2βγ before activating it, which we propose results in two distinct rates of G protein subunit dissociation.

Although cAMP binding affinities and cAR1 pre-coupling can explain the G protein dissociation rates, other factors may also contribute to the observed kinetics. Previous studies showed the presence of an intracellular pool of G proteins that undergo regulated translocation to the plasma membrane of *Dictyostelium* cells upon stimulation with higher cAMP concentrations [49,60]. The cAR1 recruitment and activation of this translocated pool of G proteins at high cAMP concentrations likely plays a role in the observed second rate of G protein dissociation. Furthermore, although cAR1 has bee extensively studied, both the pharmacology and G protein coupling of cAR1 may be more complicated than what we currently know. For instance, many mammalian GPCRs are known to form homo- or hetero-oligomers, which can affect GPCR function in different ways, including modulating ligand binding and G protein coupling [61–63]. Whether cAR1 forms dimers or higher oligomers remains to be determined but it is possible that cAMP stimulation actually alters cAR1's oligomeric state, which could then lead to inducing G protein dissociation through distinct rates. Nonetheless, our findings indicate that initial cAMP stimulation of resting *Dictyostelium* cells occurs through two distinct rates that correlate with the high and low affinity cAR1 sites. Consequently, we propose that these different signaling dynamics may play a role in initial gradient sensing. On the other hand, during chemotaxis, when cells are constantly exposed to a cAMP gradient and the heterotrimeric G protein is predicted to continuously and rapidly cycle between active and inactive states, it is possible that only uncoupled cAMP-bound cAR1 (LR) exists in this situation, cycling between LR and LRGD forms as previously proposed by Xu *et al.* [51].

4. Conclusion

We used BRET^2 to investigate the dynamics and regulation of heterotrimeric G protein Gα2βγ activation in response to cAMP stimulation in *Dictyostelium* by monitoring the dissociation of Gα2 and Gβ. Our findings indicate that cAR1 is the main receptor promoting Gα2βγ activation in both undifferentiated and 5.5 h-differentiated cells, that only very low levels of cAR1 expression are necessary to induce full activation of Gα2βγ, and suggest that caffeine increases the potency of cAMP-induced G protein subunit dissociation, although the mechanism remains unknown. In addition, our findings suggest that F-actin does not affect the coupling of cAR1 to Gα2βγ but that an intact microtubule network is necessary for efficient cAMP-induced G protein subunit activation. Finally, our kinetics analyses and receptor-G protein coupling modeling studies reveal two rates of cAMP-induced G protein subunits dislocation that highly correlate with cAR1 binding sites, leading us to propose that both uncoupled, low affinity, and Gα2βγ-coupled, high affinity, cAR1 exist in resting cells leading to the observed two rates of G protein subunit dissociation when cells are exposed to elevated cAMP concentrations. Although the study of protein-protein interactions by BRET is currently limited to measuring responses to acute stimulations, the information gained from these studies provide insights into how cells initially respond to chemoattractant exposure and into mechanisms possibly involved in sensing gradients.

Supplementary Material

Refer to Web version on PubMed Central for supplementary material.

Acknowledgments

Abbreviations

BRET	bioluminescence resonance energy transfer
cAMP	cyclic adenosine monophosphate
cAR	cAMP receptor
2'-dcAMP	2'-deoxyadenosine-5'-monophosphate
EC50	half maximal effective concentration
FRET	Förster resonance energy transfer
GD	GDP-bound heterotrimeric G protein
GFP	green fluorescent protein
GPCR	G protein-coupled receptor
GT	GTP-bound heterotrimeric G protein
L	ligand
R	receptor
***R*luc**	*Renilla* luciferase
RMSE	root mean squared error

References

[1]. Kamp ME, Liu Y, Kortholt A, Function and Regulation of Heterotrimeric G Proteins during Chemotaxis, Int. J. Mol. Sci 17 (2016) 90.

[2]. Nichols JM, Veltman D, Kay RR, Chemotaxis of a model organism: progress with Dictyostelium., Curr. Opin. Cell Biol 36 (2015) 7–12. doi:10.1016/j.ceb.2015.06.005. [PubMed: 26183444]

[3]. Chisholm RL, Firtel RA, Insights into morphogenesis from a simple developmental system, Nat. Rev. Mol. Cell Biol 5 (2004) 531–541. doi:10.1038/nrm1427. [PubMed: 15232571]

[4]. Johnson RL, Van Haastert PJM, Kimmel AR, Saxe CL, Jastorff B, Devreotes PN, The cyclic nucleotide specificity of three cAMP receptors in Dictyostelium, J. Biol. Chem 267 (1992) 4600–4607. [PubMed: 1537842]

[5]. Louis JM, Ginsburg GT, Kimmel AR, The cAMP receptor CAR4 regulates axial patterning and cellular differentiation during late development of Dictyostelium, Genes Dev 8 (1994) 2086–2096. doi:10.1101/gad.8.17.2086. [PubMed: 7958880]

[6]. Johnson RL, Saxe CL, Gollop R, Kimmel AR, Devreotes PN, Identification and targeted gene disruption of cAR3, a cAMP receptor subtype expressed during multicellular stages of

Dictyostelium development, Genes Dev 7 (1993) 273–282. doi:10.1101/gad.7.2.273. [PubMed: 8382181]

[7]. Klein PS, Sun TJ, Saxe CL, Kimmel a R., Johnson RL, Devreotes PN, A chemoattractant receptor controls development in Dictyostelium discoideum., Science 241 (1988) 1467–1472. doi: 10.1126/science.3047871. [PubMed: 3047871]

[8]. Saxe CL, Johnson RL, Devreotes PN, Kimmel AR, Expression of a cAMP receptor gene of Dictyostelium and evidence for a multigene family, Genes Dev 5 (1991) 1–8. doi:10.1101/gad. 5.1.1. [PubMed: 1989903]

[9]. Insall RH, Soede RD, Schaap P, Devreotes PN, Two cAMP receptors activate common signaling pathways in Dictyostelium., Mol. Biol. Cell 5 (1994) 703–11. doi:10.1091/mbc.5.6.703. [PubMed: 7949426]

[10]. Soede RD, Insall RH, Devreotes PN, Schaap P, Extracellular cAMP can restore development in Dictyostelium cells lacking one, but not two subtypes of early cAMP receptors (cARs). Evidence for involvement of cAR1 in aggregative gene expression., Development 120 (1994) 1997–2002. [PubMed: 7925004]

[11]. Pupillo M, Klein P, Vaughan R, Pitt G, Lilly P, Sun T, Devreotes P, Kumagai A, Firtel R, cAMP receptor and G-protein interactions control development in Dictyostelium, in: Cold Spring Harb. Symp. Quant. Biol, 1988: pp. 657–665.

[12]. Zhang N, Long Y, Devreotes PN, Ggamma in dictyostelium: its role in localization of gbetagamma to the membrane is required for chemotaxis in shallow gradients, Mol Biol Cell 12 (2001) 3204–3213. http://www.ncbi.nlm.nih.gov/entrez/query.fcgi? cmd=Retrieve&db=PubMed&dopt=Citation&list_uids=11598203. [PubMed: 11598203]

[13]. Kumagai A, Pupillo M, Gundersen R, Miake-Lye R, Devreotes PN, Firtel RA, Regulation and function of G alpha protein subunits in Dictyostelium, Cell 57 (1989) 265–275. doi:0092– 8674(89)90964–1 [pii]. [PubMed: 2539262]

[14]. Kumagai A, Hadwiger JA, Pupillo M, Firtel RA, Molecular genetic analysis of two G alpha protein subunits in Dictyostelium, J Biol Chem 266 (1991) 1220–1228. http:// www.ncbi.nlm.nih.gov/entrez/query.fcgi? cmd=Retrieve&db=PubMed&dopt=Citation&list_uids=1670774. [PubMed: 1670774]

[15]. Lilly P, Wu L, Welker DL, Devreotes PN, A G-protein beta-subunit is essential for Dictyostelium development, Genes Dev 7 (1993) 986–995. http://www.ncbi.nlm.nih.gov/entrez/query.fcgi? cmd=Retrieve&db=PubMed&dopt=Citation&list_uids=8099335. [PubMed: 8099335]

[16]. Wu L, Valkema R, Van Haastert PJM, Devreotes PN, The G protein beta subunit is essential for multiple responses to chemoattractants in Dictyostelium, J Cell Biol 129 (1995) 1667–1675. doi: 10.1083/jcb.129.6.1667. [PubMed: 7790362]

[17]. Janetopoulos C, Jin T, Devreotes P, Receptor-mediated activation of heterotrimeric G-proteins in living cells, Science (80-.). 291 (2001) 2408–2411. doi:10.1126/science.1055835291/5512/2408 [pii]. [PubMed: 11264536]

[18]. Islam AFMT, Stepanski BM, Charest PG, Studying chemoattractant signal transduction dynamics in Dictyostelium by BRET, in: Methods Mol. Biol, 2016: pp. 63–77. doi: 10.1007/978-1-4939-3480-5_5.

[19]. Hamdan FF, Percherancier Y, Breton B, Bouvier M, Monitoring protein-protein interactions in living cells by bioluminescence resonance energy transfer (BRET), Curr Protoc Neurosci Chapter 5 (2006) Unit 5 23. doi:10.1002/0471142301.ns0523s34.

[20]. Machleidt T, Woodroofe CC, Schwinn MK, Méndez J, Robers MB, Zimmerman K, Otto P, Daniels DL, Kirkland TA, Wood KV, NanoBRET-A Novel BRET Platform for the Analysis of Protein-Protein Interactions, ACS Chem. Biol 10 (2015) 1797–1804. doi:10.1021/acschembio. 5b00143. [PubMed: 26006698]

[21]. Loening AM, Fenn TD, Wu AM, Gambhir SS, Consensus guided mutagenesis of Renilla luciferase yields enhanced stability and light output, Protein Eng. Des. Sel 19 (2006) 391–400. doi:10.1093/protein/gzl023. [PubMed: 16857694]

[22]. Bertrand L, Parent S, Caron M, Legault M, Joly E, Angers S, Bouvier M, Brown M, Houle B, Menard L, The BRET2/arrestin assay in stable recombinant cells: a platform to screen

coumpounds that interact with G-protein-coupled reseptors (GPCRs), J Recept Signal Transduct Res 22 (2002) 533–41. [PubMed: 12503639]

[23]. Hereld D, Vaughan R, Kim JY, Borleis J, Devreotes P, Localization of ligand-induced phosphorylation sites to serine clusters in the C-terminal domain of the Dictyostelium cAMP receptor, cAR1, J. Biol. Chem 269 (1994) 7036–7044. [PubMed: 8120068]

[24]. Veltman DM, Akar G, Bosgraaf L, Van Haastert PJM, A new set of small, extrachromosomal expression vectors for Dictyostelium discoideum, Plasmid 61 (2009) 110–118. doi:10.1016/j.plasmid.2008.11.003. [PubMed: 19063918]

[25]. Fey P, Dodson RJ, Basu S, Chisholm RL, One stop shop for everything Dictyostelium: DictyBase and the Dicty Stock Center in 2012, Methods Mol. Biol 983 (2013) 59–92. doi:10.1007/978-1-62703-302-2-4. [PubMed: 23494302]

[26]. Octtaviani E, Effler JC, Robinson DN, Enlazin, a natural fusion of two classes of canonical cytoskeletal proteins, contributes to cytokinesis dynamics., Mol. Biol. Cell 17 (2006) 5275–86. doi:10.1091/mbc.E06-08-0767. [PubMed: 17050732]

[27]. Bastounis E, Meili R, Alonso-Latorre B, del Alamo JC, Lasheras JC, Firtel RA, The SCAR/WAVE complex is necessary for proper regulation of traction stresses during amoeboid motility, Mol. Biol. Cell 22 (2011) 3995–4003. doi:10.1091/mbc.E11-03-0278. [PubMed: 21900496]

[28]. Jeon TJ, Lee D-J, Merlot S, Weeks G, Firtel RA, Rap1 controls cell adhesion and cell motility through the regulation of myosin II, J. Cell Biol 176 (2007) 1021–1033. doi:10.1083/jcb.200607072. [PubMed: 17371831]

[29]. Sasaki AT, Chun C, Takeda K, Firtel RA, Localized Ras signaling at the leading edge regulates PI3K, cell polarity, and directional cell movement, J Cell Biol 167 (2004) 505–518. [PubMed: 15534002]

[30]. Huang YE, Iijima M, Parent CA, Funamoto S, Firtel RA, Devreotes P, Receptor-mediated regulation of PI3Ks confines PI(3,4,5)P3 to the leading edge of chemotaxing cells, Mol Biol Cell 14 (2003) 1913–1922. http://www.ncbi.nlm.nih.gov/entrez/query.fcgi?cmd=Retrieve&db=PubMed&dopt=Citation&list_uids=12802064. [PubMed: 12802064]

[31]. Julia Sun T, Devreotes PN, Gene targeting of the aggregation stage cAMP receptor cAR1 in Dictyostelium, Genes Dev 5 (1991) 572–582. doi:10.1101/gad.5.4.572. [PubMed: 1849108]

[32]. Kim JY, Soede RDM, Schaap P, Valkema R, Borleis JA, Van Haastert PJM, Devreotes PN, Hereld D, Phosphorylation of chemoattractant receptors is not essential for chemotaxis or termination of G-protein-mediated responses, J. Biol. Chem 272 (1997) 27313–27318. doi:10.1074/jbc.272.43.27313. [PubMed: 9341180]

[33]. Bader S, Kortholt A, Van Haastert PJ, Seven Dictyostelium discoideum phosphodiesterases degrade three pools of cAMP and cGMP, Biochem J 402 (2007) 153–161. http://www.ncbi.nlm.nih.gov/entrez/query.fcgi?cmd=Retrieve&db=PubMed&dopt=Citation&list_uids=17040207. [PubMed: 17040207]

[34]. Takeda K, Shao D, Adler M, Charest PG, Loomis WF, Levine H, Groisman A, Rappel WJ, Firtel RA, Incoherent feedforward control governs adaptation of activated ras in a eukaryotic chemotaxis pathway, Sci Signal 5 (2012) ra2. doi:10.1126/scisignal.2002413. [PubMed: 22215733]

[35]. Skoge M, Yue H, Erickstad M, Bae A, Levine H, Groisman A, Loomis WF, Rappel W-J, Cellular memory in eukaryotic chemotaxis, Proc. Natl. Acad. Sci 111 (2014) 14448–14453. doi:10.1073/pnas.1412197111. [PubMed: 25249632]

[36]. Engel R, Van Haastert PJM, Visser AJWG, Spectral characterization of Dictyostelium autofluorescence, Microsc. Res. Tech 69 (2006) 168–174. doi:10.1002/jemt.20282. [PubMed: 16538623]

[37]. Bloomfield G, Superoxide signalling required for multicellular development of Dictyostelium, J. Cell Sci 116 (2003) 3387–3397. doi:10.1242/jcs.00649. [PubMed: 12840076]

[38]. Johnson RL, Caterina MJ, Devreotes PN, Van Haastert PJM, Vaughan RA, Overexpression of the cAMP Receptor 1 in Growing Dictyostelium Cells, Biochemistry 30 (1991) 6982–6986. doi:10.1021/bi00242a025. [PubMed: 1648967]

[39]. Klein C, Juliani MH, cAMP-induced changes in cAMP-binding sites on D. discoideum amebae, Cell. 10 (1977) 329–335. doi:10.1016/0092-8674(77)90227-6. [PubMed: 189939]

[40]. Van Haastert PJM, De Wit RJW, Demonstration of receptor heterogeneity and affinity modulation by nonequilibrium binding experiments. The cell surface cAMP receptor of Dictyostelium discoideum, J. Biol. Chem 259 (1984) 13231–13328.

[41]. Brenner M, Thoms SD, Caffeine blocks activation of cyclic AMP synthesis in Dictyostelium discoideum, Dev Biol 101 (1984) 136–146. doi:0012–1606(84)90124–6 [pii]. [PubMed: 6319207]

[42]. Liao XH, Buggey J, Lee YK, Kimmel AR, Chemoattractant Stimulation of TORC2 is Regulated by Receptor/G protein Targeted Inhibitory Mechanisms that Function Upstream and Independently of an Essential GEF/Ras Activation Pathway in Dictyostelium, Mol Biol Cell (2013). doi:10.1091/mbc.E13-03-0130.

[43]. Kumagai a, Hadwiger J. a, Pupillo M, R. a Firtel, Molecular genetic analysis of two G alpha protein subunits in Dictyostelium., J. Biol. Chem 266 (1991) 1220–8. http://www.ncbi.nlm.nih.gov/pubmed/1670774. [PubMed: 1670774]

[44]. Rot G, Parikh A, Curk T, Kuspa A, Shaulsky G, Zupan B, dictyExpress: a Dictyostelium discoideum gene expression database with an explorative data analysis web-based interface., BMC Bioinformatics 10 (2009) 265. doi:10.1186/1471-2105-10-265. [PubMed: 19706156]

[45]. de Keijzer S, Galloway J, Harms GS, Devreotes PN, Iglesias PA, Disrupting microtubule network immobilizes amoeboid chemotactic receptor in the plasma membrane, Biochim. Biophys. Acta 1808 (2011) 1701–1708. doi:10.1016/j.bbamem.2011.02.009. [PubMed: 21334306]

[46]. Janetopoulos C, Ma L, Devreotes PN, Iglesias PA, Chemoattractant-induced phosphatidylinositol 3,4,5-trisphosphate accumulation is spatially amplified and adapts, independent of the actin cytoskeleton, Proc. Natl. Acad. Sci 101 (2004) 8951–8956. doi:10.1073/pnas.0402152101. [PubMed: 15184679]

[47]. Davidse LC, Benzimidazole Fungicides: Mechanism of Action and Biological Impact, Annu. Rev. Phytopathol 24 (1986) 43–65. doi:10.1146/annurev.py.24.090186.000355.

[48]. Welker DL, Williams KL, Mitotic Arrest and Chromosome Doubling Using Thiabendazole, Cambendazole, Nocodazole and Ben Late in the Slime Mould Dictyostelium discoideum, Microbiology 116 (1980) 397–407. doi:10.1099/00221287-116-2-397.

[49]. Elzie CA, Colby J, Sammons MA, Janetopoulos C, Dynamic localization of G proteins in Dictyostelium discoideum, J Cell Sci 122 (2009) 2597–2603. doi:10.1242/jcs.046300. [PubMed: 19584094]

[50]. Xu X, Meier-Schellersheim M, Jiao X, Nelson LE, Jin T, Quantitative Imaging of Single Live Cells Reveals Spatiotemporal Dynamics of Multistep Signaling Events of Chemoattractant Gradient Sensing in Dictyostelium, Mol. Biol. Cell 16 (2005) 676–688. doi:10.1091/mbc.E04-07-0544. [PubMed: 15563608]

[51]. Xu X, Meckel T, Brzostowski JA, Yan J, Meier-Schellersheim M, Jin T, Coupling Mechanism of a GPCR and a Heterotrimeric G Protein During Chemoattractant Gradient Sensing in Dictyostelium, Sci Signal 3 (2010) ra71 doi:3/141/ra71 [pii]10.1126/scisignal.2000980. [PubMed: 20876874]

[52]. Gales C, V Rebois R, Hogue M, Trieu P, Breit A, Hebert TE, Bouvier M, Real-time monitoring of receptor and G-protein interactions in living cells, Nat Methods 2 (2005) 177–184. doi:nmeth743 [pii]10.1038/nmeth743. [PubMed: 15782186]

[53]. Gales C, Van Durm JJ, Schaak S, Pontier S, Percherancier Y, Audet M, Paris H, Bouvier M, Probing the activation-promoted structural rearrangements in preassembled receptor-G protein complexes, Nat Struct Mol Biol 13 (2006) 778–786. 10.1038/nsmb1134. [PubMed: 16906158]

[54]. Whorton MR, Bokoch MP, Rasmussen SGF, Huang B, Zare RN, Kobilka B, Sunahara RK, A monomeric G protein-coupled receptor isolated in a high-density lipoprotein particle efficiently activates its G protein, Proc. Natl. Acad. Sci 104 (2007) 7682–7687. doi:10.1073/pnas.0611448104. [PubMed: 17452637]

[55]. Nobles M, Benians A, Tinker A, Heterotrimeric G proteins precouple with G protein-coupled receptors in living cells., Proc. Natl. Acad. Sci. U. S. A 102 (2005) 18706–18711. doi:10.1073/pnas.0504778102. [PubMed: 16352729]

[56]. Philip F, Sengupta P, Scarlata S, Signaling through a G protein-coupled receptor and its corresponding G protein follows a stoichiometrically limited model, J. Biol. Chem 282 (2007) 19203–19216. doi:10.1074/jbc.M701558200. [PubMed: 17420253]

[57]. Janssens PMW, van der Geer PLJ, Arents JC, van Driel R, Guanine nucleotides modulate the function of chemotactic cyclic AMP receptors in Dictyostelium discoideum, Mol. Cell. Biochem 67 (1985) 119–124. doi:10.1007/BF02370170. [PubMed: 2995788]

[58]. Schenk PW, Van Es S, Kesbeke F, Snaar-Jagalska BE, Involvement of cyclic AMP cell surface receptors and G-proteins in signal transduction during slug migration of Dictyostelium discoideum, Dev. Biol 145 (1991) 110–118. doi:10.1016/0012-1606(91)90217-Q. [PubMed: 1850366]

[59]. van Hemert F, Lazova MD, Snaar-Jagaska BE, Schmidt T, Mobility of G proteins is heterogeneous and polarized during chemotaxis, J Cell Sci 123 (2010) 2922–2930. doi:jcs. 063990 [pii]10.1242/jcs.063990. [PubMed: 20682639]

[60]. Kamimura Y, Miyanaga Y, Ueda M, Heterotrimeric G-protein shuttling via Gip1 extends the dynamic range of eukaryotic chemotaxis, Proc. Natl. Acad. Sci 113 (2016) 4356–4361. doi: 10.1073/pnas.1516767113. [PubMed: 27044073]

[61]. Park PS-H, Lodowski DT, Palczewski K, Activation of G Protein–Coupled Receptors: Beyond Two-State Models and Tertiary Conformational Changes, Annu. Rev. Pharmacol. Toxicol 48 (2008) 107–141. doi:10.1146/annurev.pharmtox.48.113006.094630. [PubMed: 17848137]

[62]. Ferre S, Casado V, Devi LA, Filizola M, Jockers R, Lohse MJ, Milligan G, Pin J-P, Guitart X, G Protein-Coupled Receptor Oligomerization Revisited: Functional and Pharmacological Perspectives, Pharmacol. Rev 66 (2014) 413–434. doi:10.1124/pr.113.008052. [PubMed: 24515647]

[63]. Gahbauer S, Böckmann RA, Membrane-mediated oligomerization of G protein coupled receptors and its implications for GPCR function, Front. Physiol 7 (2016). doi:10.3389/fphys.2016.00494.

Article highlights

- cAMP induces cAR1-mediated G protein activation to a similar extent in both undifferentiated and 5.5 h-differentiated *Dictyostelium* cells.

- Caffeine increases the potency of cAMP-induced Gα2βγ activation.

- An intact microtubule network and not F-actin is necessary for efficient cAMP-induced Gα2βγ activation.

- Kinetic analyses and quantitative modeling suggest that both uncoupled and pre-coupled cAR1-Gα2βγ contribute to the response of cells stimulated by elevated cAMP concentrations through different kinetics.
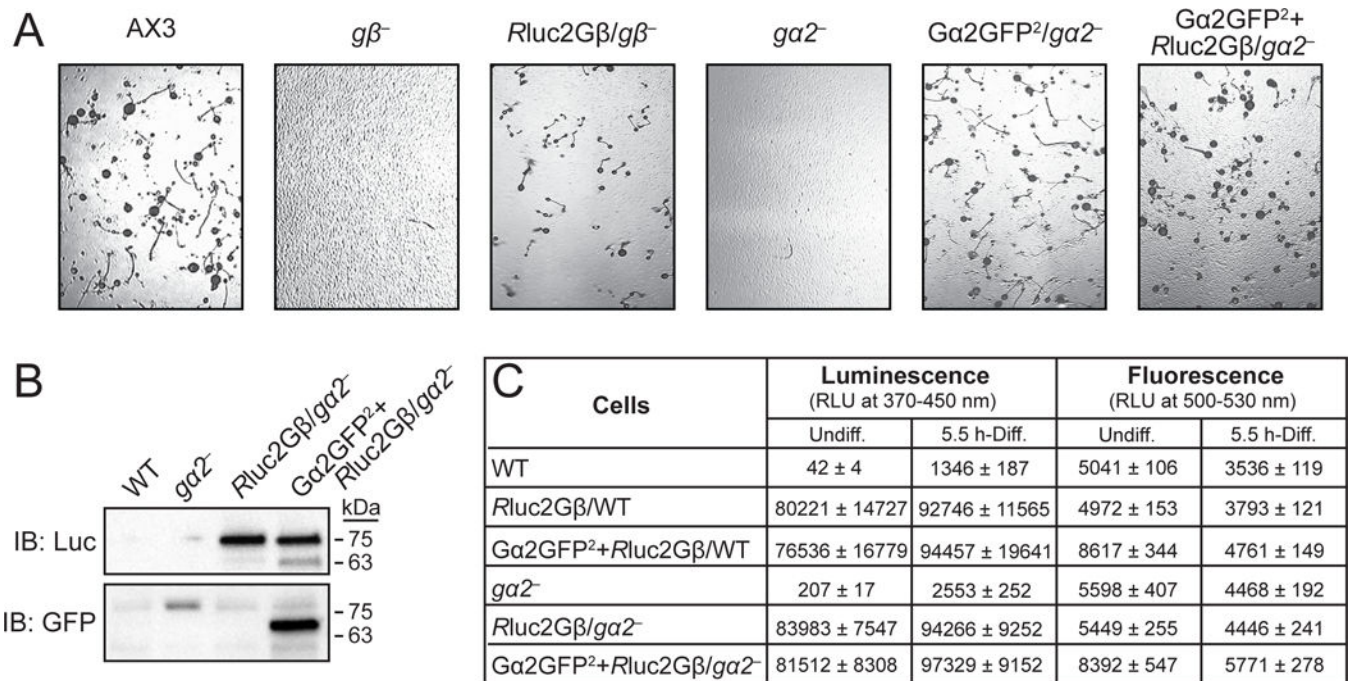
Fig. 1. Validation of *R*luc2Gβ and Gα2GFP² fusion constructs.
A, Pictures show the morphological phenotype of developing cells at 24 h after initial plating on non-nutrient agar. B, Expression of *R*luc2Gβ and Gα2GFP² in cells lacking Gα2 (*ga2⁻*). Immunoblots (IB) using anti-GFP and anti-Renilla Luciferase (Luc) antibodies are shown. Wild-type (WT) cells and *ga2⁻* cells were used as control. C, Measurements of luminescence at 370–450 nm, produced upon addition of coelenterazine h, and fluorescence at 500–530 nm, produced upon excitation of the samples at 450–470 nm. Luminescence and fluorescence are reported in relative light units (RLU) for WT and *ga2⁻* cells (background levels), and cells expressing *R*luc2Gβ alone or together with Gα2GFP². The errors represent standard deviation. Results are expressed as the mean or are representative of at least three independent experiments.
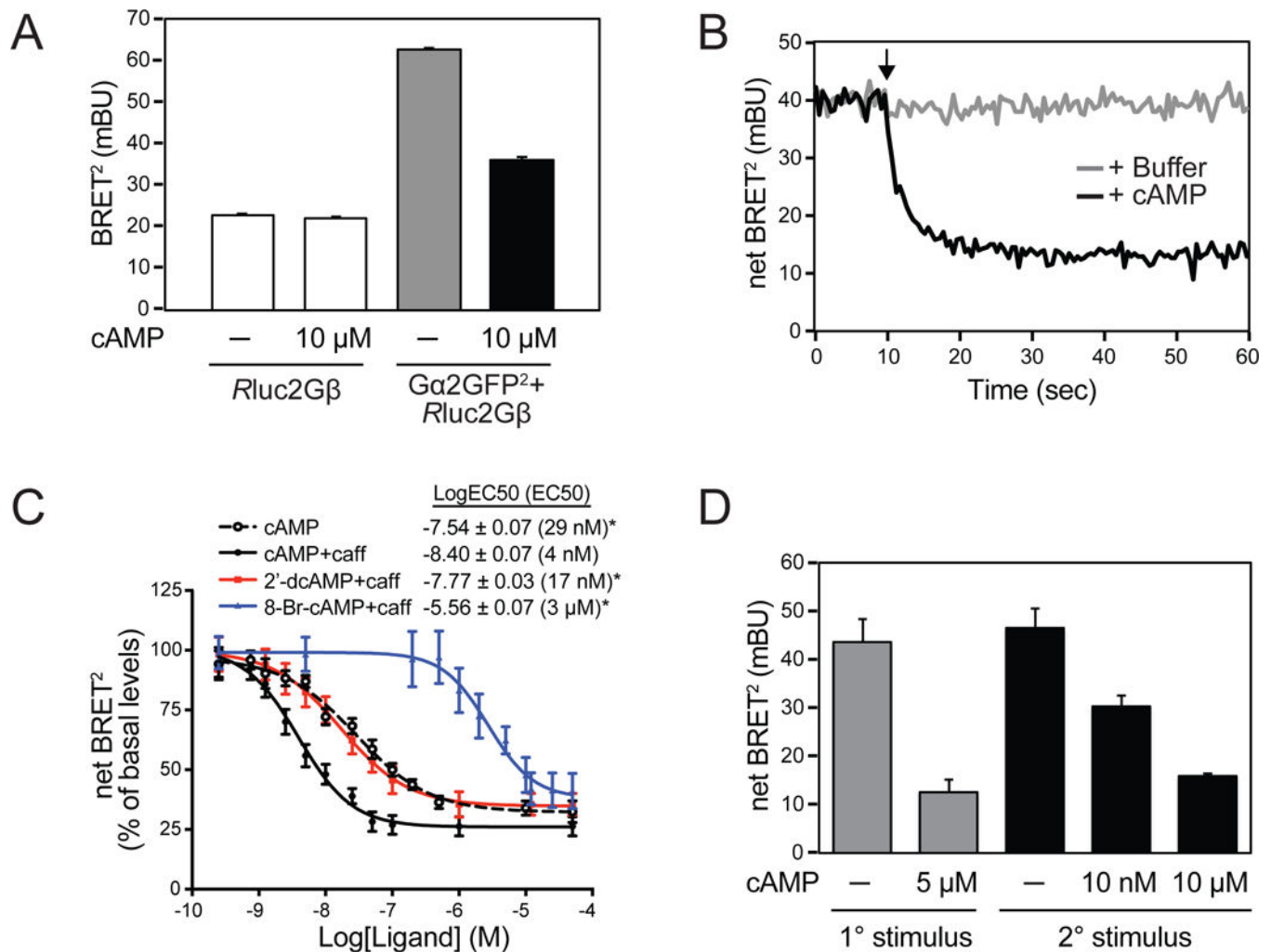
Fig. 2. Gα2βγ subunits dissociation detected by BRET^2 reflects activation.
A, BRET^2 measurements obtained from $ga2^-$ cells expressing Rluc2Gβ alone or together with Gα2GFP^2 before and after 1 min stimulation with 10 μM cAMP. Error bars represent the standard deviation. B, Representative net BRET^2 values obtained from measurements taken continuously every 0.5 s before, during and after injection of either buffer as control or 10 μM cAMP to Gα2GFP^2/Rluc2Gβ/$ga2^-$ cells. Solid arrow indicates stimulus injection. C, Net BRET^2 values for Gα2GFP^2/Rluc2Gβ/$ga2^-$ cells stimulated with different concentrations of the indicated cAR1 ligands, expressed as % of the net BRET^2 levels in non-stimulated cells. cAMP dose-responses were measured in the presence (+caff) and absence of 5 mM caffeine. LogEC50 (effective concentration of ligand producing 50% of the maximal stimulation) values are indicated with their standard errors, and EC50 values are indicated in parentheses, for each ligand and condition. Error bars represent the standard error. * $p < 0.0001$. D, Net BRET^2 values before and after a first stimulation of Gα2GFP^2/ Rluc2Gβ/$ga2^-$ cells with 5 μM cAMP are indicated under 1° stimulus. One min after the first stimulus, cells were washed twice with 12 mM Na/K phosphate buffer and the net BRET^2 of the same cells was measured again before and after stimulation with 10 nM or 10

μM cAMP (2° stimulus). Error bars represent the standard deviation. mBU, milli BRET^2 units. Results are expressed as the mean of at least three independent experiments.
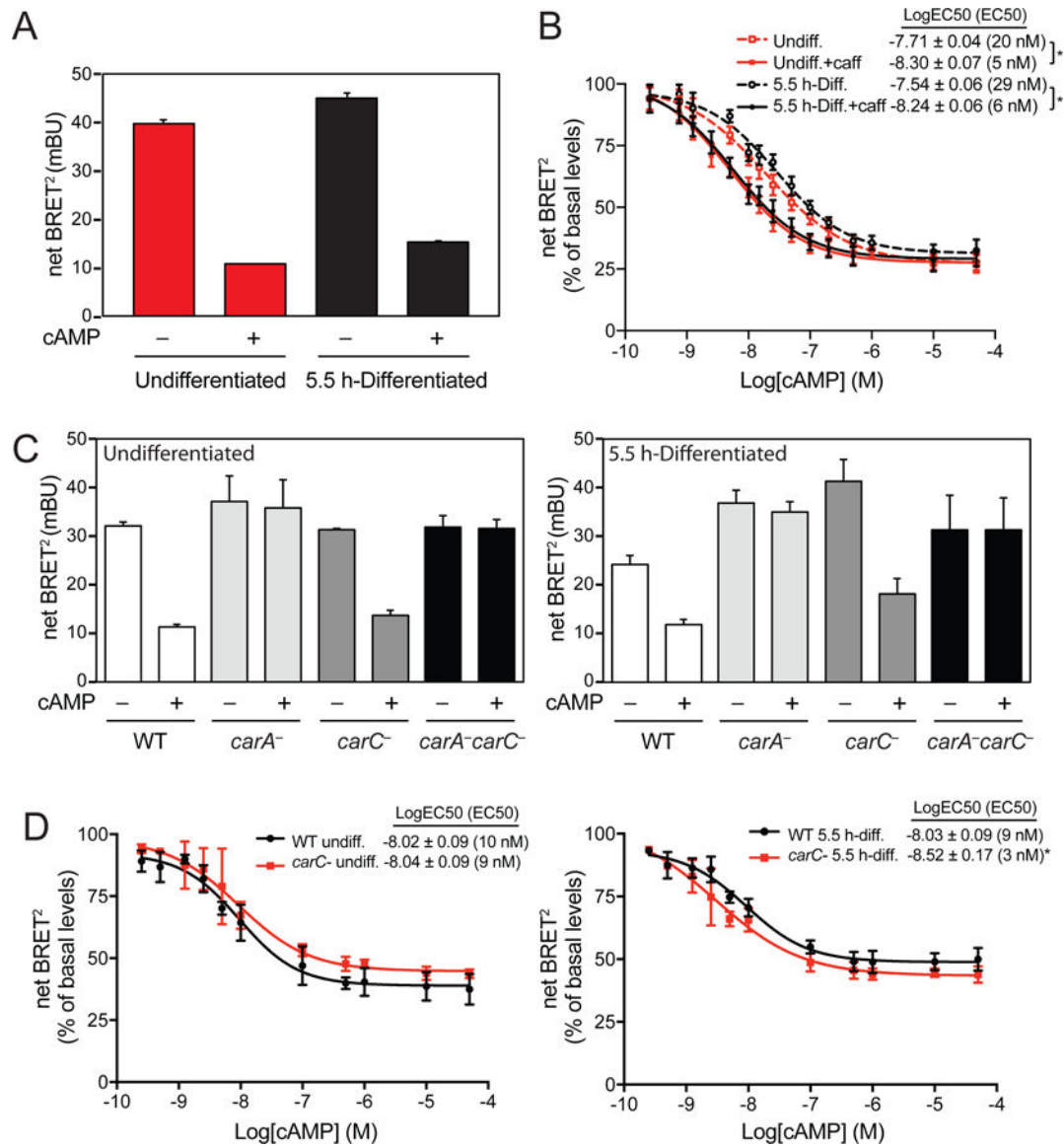
Fig. 3. cAR1-induced Gα2βγ subunits dissociation in undifferentiated and 5.5 h-differentiated cells.

A, Net BRET^2 values for measurements obtained before and after 10 μM cAMP stimulation of undifferentiated and 5.5 h-differentiated Gα2GFP^2/Rluc2Gβ/*ga2*⁻ cells. B, Net BRET^2 values for measurements obtained of Gα2GFP^2/Rluc2Gβ/*ga2*⁻ cells stimulated with different cAMP concentrations, expressed as % of the net BRET^2 levels in non-stimulated cells. LogEC50 values are indicated with their standard errors, EC50 values are indicated in parentheses. * $p < 0.001$. C, Net BRET^2 values for measurements obtained of undifferentiated and 5.5 h-differentiated wild-type (WT) cells and cells lacking cAR1 (*carA*⁻), cAR3 (*carC*⁻) or both cAR1 and cAR3 (*carA*⁻*carC*⁻), expressing Gα2GFP^2 and Rluc2Gβ before and after stimulation with 10 μM cAMP. D, Net BRET^2 values for measurements obtained of WT and *carC*⁻ cells expressing Gα2GFP^2 and Rluc2Gβ stimulated with different cAMP concentrations, expressed as % of the net BRET^2 levels in non-stimulated cells. LogEC50 values are indicated with their standard errors, EC50 values

are indicated in parentheses. * $p < 0.05$. Results are expressed as the mean of at least three independent experiments. Error bars represent the standard deviation in bar graphs and standard error in dose-response curves.
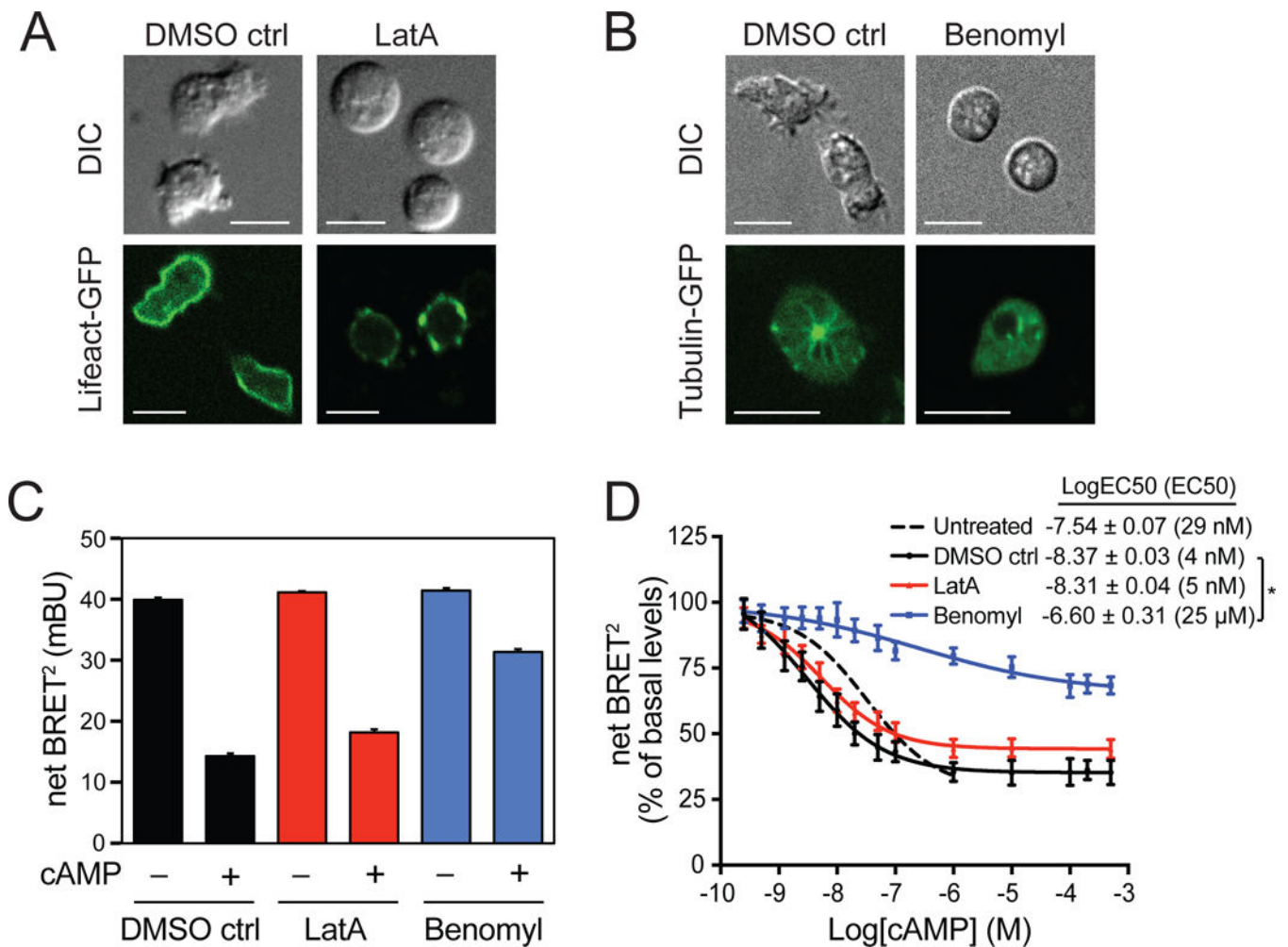
Fig. 4. The role of F-actin and microtubules in cAMP-induced Gα2βγ subunits dissociation.
A, Differential interference contrast (DIC) and Lifeact-GFP fluorescence confocal images of 5.5 h-differentiated wild-type cells treated either with 0.5 % DMSO (vehicle control) or 5 μM Latrunculin A (LatA) for 15 min. B, DIC and Tubulin-GFP fluorescence confocal images of 5.5 h-differentiated wild-type cells treated either with 0.5 % DMSO (vehicle control) or 50 μM Benomyl for 15 min. C, Net $BRET^2$ values for measurements obtained before and after 10 μM cAMP stimulation of 5.5 h-differentiated Gα2GFP^2/Rluc2Gβ/$ga2^-$ cells pretreated with 0.5 % DMSO as control, 5 μM LatA or 50 μM Benomyl for 15 min. D, Net $BRET^2$ values for measurements obtained with Gα2GFP^2/Rluc2Gβ/$ga2^-$ cells pretreated with 0.5 % DMSO as control, 5 μM LatA or 50 μM Benomyl for 15 min, and stimulated with different cAMP concentrations. Data are expressed as % of the net $BRET^2$ levels in non-stimulated cells. LogEC50 values are indicated with their standard errors, EC50 values are indicated in parentheses. * $p < 0.001$. Results are expressed as the mean or are representative of at least three independent experiments. Error bars represent the standard deviation for the bar graph and standard error for the dose-response curves.
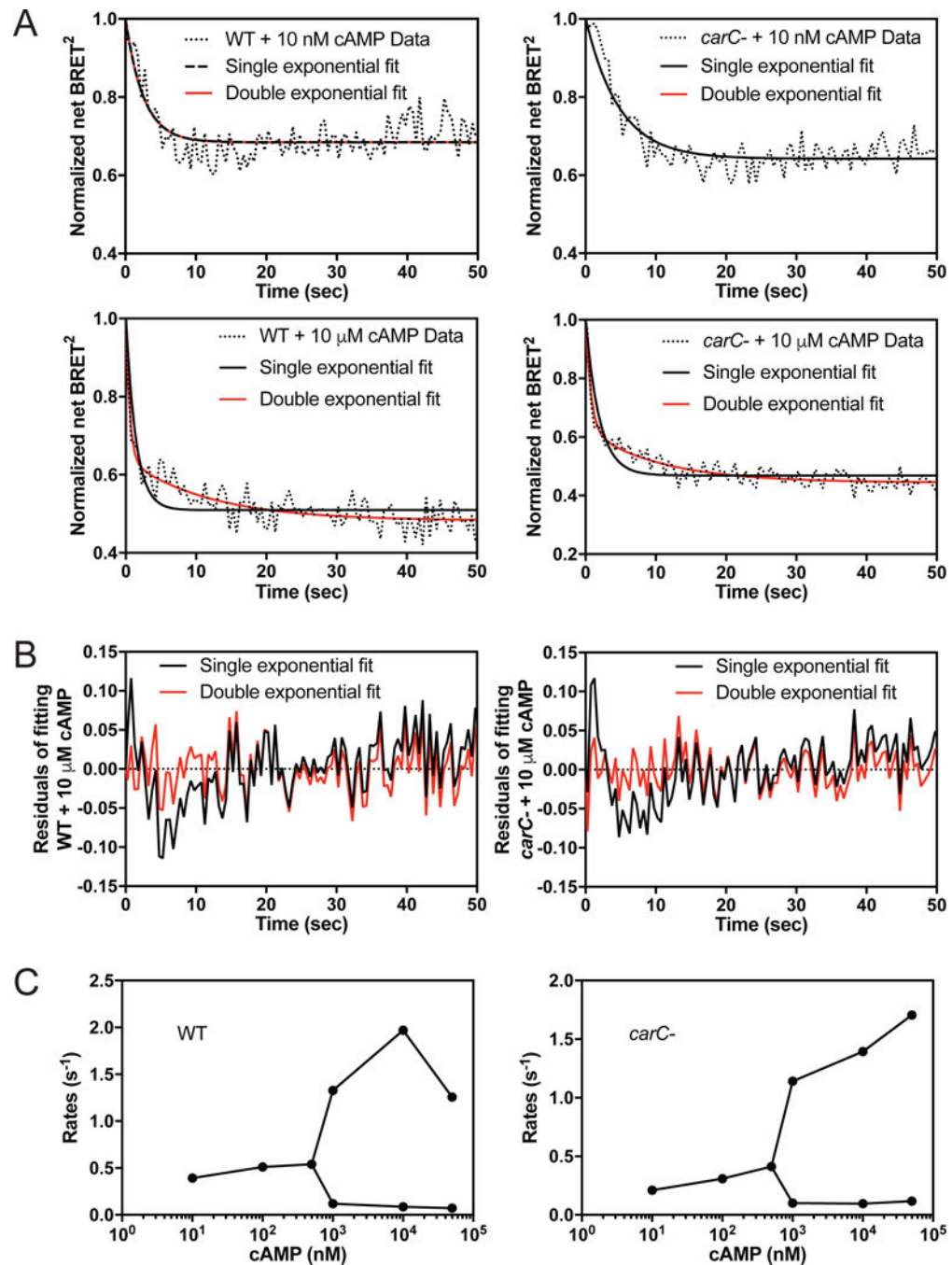
Fig. 5. Kinetics analyses of cAMP-induced Gα2βγ subunits dissociation.
A, Net BRET^2 values for measurements taken every 0.5 s after stimulation of wild-type (WT) cells and *carC*$^-$ cells expressing Gα2GFP^2 and *R*luc2Gβ with 10 nM or 10 μM cAMP, normalized to net BRET^2 levels before stimulation. The curves were fitted using single and double exponential functions. For the 10 nM data, the fits are identical and overlap. B, Residuals for single and double exponential fittings for the 10 μM cAMP-stimulated conditions shown in A were calculated by subtracting the measured values from the fitted values. C, Rates of Gα2βγ subunits dissociation determined from the time curve fittings

obtained for 10 nM, 100 nM, 500 nM, 1 μM, 10 μM, and 50 μM cAMP stimulations of WT and *carC*⁻ cells. Results represent the mean or the analyses of at least three independent experiments.
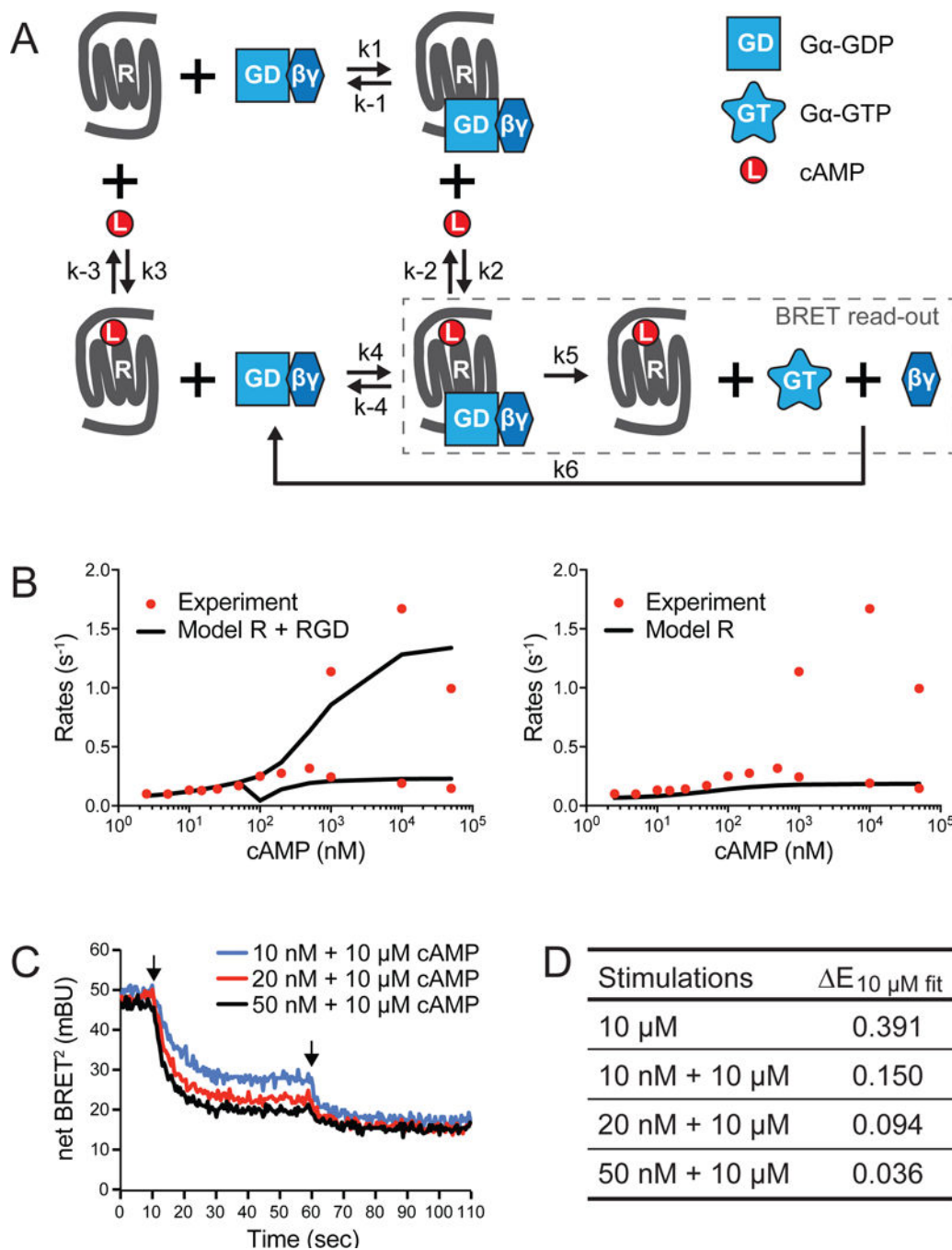
Fig. 6. Quantitative modeling of the observed Gα2βγ subunits dissociation kinetics.
A, Conceptual model of cAR1-Gα2βγ coupling. The constants are defined in the Materials and Methods section. B, Rates of Gα2βγ subunits dissociation induced by different concentrations of cAMP obtained from analyzing the experimental data for wild-type cells from Fig. 5C (red circles) and from quantitatively modeling the responses where both uncoupled (R) and pre-coupled (RGD) cAR1 bind the cAMP ligand (L) or where only uncoupled cAR1 is present and mediates the response to cAMP (black curves). C, Representative net BRET^2 values obtained from measurements taken continuously every 0.5

s before, during and after injection of a first cAMP stimulus of 10, 20, or 50 nM at 10 s, and of a second cAMP stimulus of 10 μM at 60 s of Gα2GFP^2/Rluc2Gβ/$ga2^-$ cells. Solid arrows indicate when the cAMP stimuli were injected. D, Calculated error differences (E) for single and double exponential fittings of the Gα2βγ subunits dissociation kinetics induced by 10 μM cAMP stimulation alone (from data presented in Fig. 5A) or after the first stimuli indicated in C. E calculations and interpretations are described in the Materials and Methods section and main text. Results represent the mean or the analyses of at least three independent experiments.